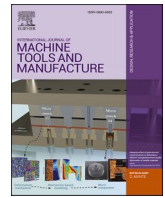# The effects of grit properties and dressing on grinding mechanics and wheel performance: Analytical assessment framework

N.B. When citing this work, cite the original published paper.

(article starts on next page)

The effects of grit properties and dressing on grinding mechanics and wheel performance: Analytical assessment framework

Nastja Macerol [a,b,*], Luiz F.P. Franca [a], Radovan Drazumeric [c], Peter Krajnik [b]

[a] *Element Six (UK) Ltd., Global Innovation Centre, Didcot, United Kingdom*
[b] *Chalmers University of Technology, Department of Industrial and Materials Science, Gothenburg, Sweden*
[c] *University of Ljubljana, Faculty of Mechanical Engineering, Ljubljana, Slovenia*

A B S T R A C T

This paper introduces an analytical assessment framework for evaluating grinding wheel performance derived from the model of cutting and sliding grinding force components. Four new parameters are proposed based on wheel topography. These parameters are normalized through the aggressiveness number, which circumvents the influences of grinding geometry and kinematics. The framework is validated through experiments with different wheel topographies obtained by changing dressing conditions and grit properties (toughness, thermal stability and shape). The framework and experiments quantify how wheel wear flat area influences the sliding component and how grit protrusion influences the intrinsic specific grinding energy. This framework provides a rational basis for evaluating grinding-wheel performance and abrasive-grit selection.

1. Introduction

During grinding, the process geometry, kinematics and, in particular, the grinding-wheel topography all have a strong influence on the material-removal mechanisms and, consequently, process outputs such as forces, heat generation, wheel wear and workpiece surface topography.

One critical factor that influences the wheel topography is the bond type. Electroplated or single-layer tools generally have a rougher grinding-wheel surface and more-pronounced grit protrusion compared to dressed resin- and vitrified-bonded multilayer tools. This is primarily due to single-layer tool's lack of truing. However, even trued and dressed wheels can exhibit vast difference in wheel macro- and micro-topography based on grit types and truing/dressing parameters. Although previous studies have considered the effects of truing/dressing parameters on grinding [1], the specific properties of grits and bonds and their effect on wheel topography are seldom used in these assessments.

Malkin and Cook investigated wheel-wear mechanisms [2,3] and the relationship between one of those mechanisms, wear-flats at the grain tips, and forces during grinding [2]. Using various analysis methods, Cai and Rowe proposed four parameters that can quantify grinding-wheel topography: active cutting-edge density, cutting-edge dullness, effective porosity volume, and wheel scratch hardness [4]. Badger and Torrance proposed a model based on a normal distribution of cutting asperities assuming pyramidal-shaped grits [5] and then correlated the model with grinding forces for various dressing conditions. Nguyen and Butler used the density and sharpness of abrasive grains and the coarseness of the wheel to predict grinding performance [6]. Other researches have taken a different approach: generating uniform grain-like features on the grinding wheel and thus controlling the surface topography [7] in an attempt to achieve a predictable grinding process. In most of the above studies, the reason for quantifying the wheel topography was to predict grinding performance.

Shih evaluated vitrified-bonded cBN, diamond and SiC tools when grinding ceramics and found that grit properties greatly affected performance [8]. Hitchiner et al. showed the influence of grit properties and bond strength when grinding with cBN grits of variable toughness under fixed dressing conditions [9]. Palmer et al. evaluated different engineered-shape grains with conventional abrasives under various dressing conditions [10] and found that an elongated grit generates the largest workpiece R_a surface roughness, which they attributed to an increased penetration depth. While the research about the influence of grit and bond properties on grinding performance is clear, particularly with regard to grit wear, little work has been done on how these same properties influence the grinding-wheel topography, which is the fundamental causal mechanism for differences in grinding performance.

Nomenclature

A	wheel wear flat area in percent
A_{sl}	wheel wear flat area in mm^2
A_c	cross-sectional area
α	wheel contact area
$\Delta\alpha$	grit protrusion
a_{ed}	depth of dress
a_e	depth of cut
a_{pd}	active width of dresser
AR	aspect ratio of the grit particle
$Aggr$	grinding aggressiveness-number
$Aggr_D$	dressing aggressiveness-number
$Aggr_0$	transition aggressiveness-number
b	grinding width (width of cut)
c	shortest cord of the 2D projection of the grit
cBN	cubic Boron Nitride
d_e	equivalent wheel diameter
d	longest Feret diameter of the 2D projection of the grit
D10	10% of volume of particles below measured size and shape
D50	50% of volume of particles below measured size and shape
D90	90% of volume of particles below measured size and shape
e^*	intrinsic specific grinding energy
e	total specific grinding energy
$\boldsymbol{F}$	grinding force vector
$\boldsymbol{F}_c$	cutting force vector
F^n	normal force component
$\boldsymbol{F}_{sl}$	sliding force vector
F^t	tangential force component
F^n_c	normal component of cutting force
F^t_c	tangential component of cutting force
F^n_{sl}	normal component of sliding force
F^t_{sl}	tangential component of sliding force
f_{ad}	crossfeed velocity in dressing
h_{eq}	equivalent chip-thickness
i_d	collision number
l_c	wheel-workpiece contact length
P	grinding power
$\bar{p}$	average contact pressure between wheel wear flat and workpiece
$Q^{'}$	specific material-removal rate
q	dressing speed ratio
SiC	Silicon carbide
TI	toughness index
TS	thermal stability
U_d	dressing overlap ratio
v_r	dresser speed
v_s	wheel speed
v_w	workpiece speed
δ	interference angle
ξ	cutting force ratio
μ	friction coefficient
σ	normal stress
τ	tangential stress
τ_0	sliding component of tangential stress

Dressing is a crucial part of the grinding process because it enables modification of wheel surface to achieve a desirable grinding action. Brinksmeier and Cinar developed the parameter the *collision number* (i_d), which correlated with the grit flatness and, consequently, the grinding forces [11]. Malkin and Murray examined the *interference angle* (δ) [12], showing that a larger interference angle produces a sharper wheel and, consequently, lower grinding forces and larger values of workpiece R_a surface roughness [13]. The dressing aggressiveness ($Aggr_D$) was used to quantify the intensity of the abrasive interaction between the dresser and the grinding wheel [14], with a larger aggressiveness producing lower grinding forces and larger R_a values. While the interference angle δ is derived from a geometrical perspective, i.e. the angle at which a diamond attacks the grit in its trochoidal path in rotary dressing [12], the dressing aggressiveness $Aggr_D$ is derived from the kinematics, i.e. the ratio of the normal to tangential component of the relative velocity vectors [14].

While the effect of dressing parameters on wheel sharpness and grinding outputs has been well researched for a given grit-bond combination, the effect of grit type, bond type, grit properties and bond properties on dressing action has not. Indeed, different bonds and grit and bond properties all react differently to a given set of dressing conditions [10]. Therefore, one of the main objectives of this work is to develop an assessment framework for evaluating the performance of grinding wheels that can capture the effects of grinding wheel topography, with a special focus on the influence of grit type, grit properties and dressing conditions.

Traditionally, investigations into grinding processes have involved plotting relationships such as F vs A (forces vs. wheel wear-flat area) [2], e vs Q' (specific energy vs. specific material removal rate) [15,16], P vs Q' (power vs. specific material removal rate) [15,17] and e vs $Aggr$ (specific energy vs. aggressiveness) [14,16,18]. However, these basic plots generally do not include parameters that could be used for evaluation of the effects of grinding-wheel topography. To facilitate such an extension, the wheel-workpiece interface laws are initially built upon

the established models of Malkin and Cook for cutting and sliding force components [2]. Also, instead of power derivations [17], a first-principles approach is taken to obtain the stress relationships in the abrasive contact. By removing the effects of process geometry and kinematics via the use of the aggressiveness number, the effect of different grit types and dressing conditions on grinding-wheel topography can be evaluated. For example, the effects of grit protrusion and wear-flat area are correlated to grinding performance indicators such as the intrinsic specific grinding energy, the sliding component of tangential stress, the force ratio, and the friction coefficient. This concept is described and discussed in Section 5 – the experimental proof-of-concept – and is concerned with different grit properties and dressing conditions. The framework presented here is applied to conventional grinding with a rigid grinding wheel. However, the accounting of grit properties could be extended to compliant grinding using flexible/elastic tools [19] or any abrasive process where the dominant removal mechanism is chip formation.

2. Theory

2.1. Wheel-workpiece interface laws

Malkin and Cook [2] divided the contact acting at the grit-workpiece interface into two independent components: (i) cutting (or shearing), and (ii) rubbing and ploughing (which is often referred to simply as sliding). Therefore, as shown in Fig. 1, the total force $\boldsymbol{F}$ can be divided into two components, one due to cutting ($\boldsymbol{F}_c$) and one due to sliding ($\boldsymbol{F}_{sl}$):

$$\boldsymbol{F} = \boldsymbol{F}_c + \boldsymbol{F}_{sl} \tag{1}$$

The sliding component is defined as the amount of rubbing and ploughing in the area of contact between the wear flats and workpiece. At zero wear-flat area, the sliding force is zero and the grinding force is equal to the cutting force. The magnitude of the cutting force component
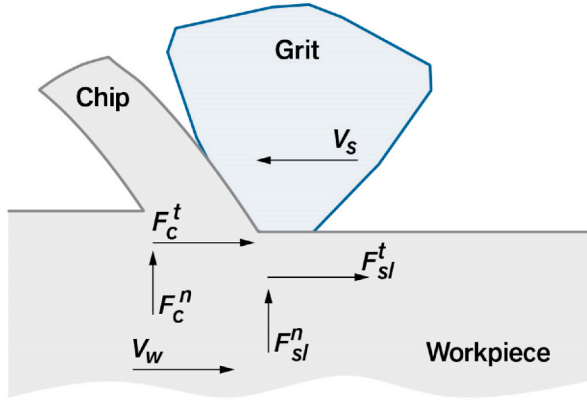
Fig. 1. Schematic illustration of chip formation. The cutting and sliding force components are shown (adapted from Malkin and Cook's investigation into attritious wear in grinding [2], where an abrasive grit develops a flat area due to rubbing against the workpiece surface).

F_c is proportional to the cross-sectional cutting area, which can be expressed as $A_c = h_{eq}b$. The tangential and normal components of cutting force (see Fig. 1) can be expressed as:

$$F_c{}^t = e^* A_c \tag{2}$$

$$F_c{}^n = \frac{e^*}{\xi} A_c \tag{3}$$

where e^* (J/mm^3) represents the intrinsic specific grinding energy, defined as the energy required to remove a unit volume of material for a given wheel topography and workpiece. Note that the above e^* is not equal to minimum specific grinding energy related to workpiece material melting energy [15,20]. The ratio $\xi = F_c{}^t/F_c{}^n$ is the cutting-force ratio [2], h_{eq} is the equivalent chip thickness (defined by Snoeys and Peters in Ref. [21]), and b the width of grinding.

It is important to note that the equivalent chip thickness, does not account for the contact length l_c. Therefore, to fully incorporate the geometrical effect on the process, the aggressiveness number ($Aggr$) is used as a fundamental, dimensionless parameter, where $Aggr = h_{eq}/l_c$. As a result, A_c can be expressed as $A_c = Aggr \cdot l_c \cdot b$.

While much work has been done investigating the cutting component, a limited number of investigations has been devoted to studying the sliding components, which can be expressed as:

$$F_{sl}^t = \mu \bar{p} A_{sl} \tag{4}$$

$$F_{sl}^n = \bar{p} A_{sl} \tag{5}$$

where μ is the friction coefficient at the grit-workpiece interface, $\bar{p}$ is the average contact pressure between the wear flat and workpiece, and A_{sl} is the wheel wear flat area in mm^2, with $A_{sl} = A l_c b$, where A is the wheel wear-flat area expressed in percent. Based on experimental observations by Malkin and Cook [2], μ and $\bar{p}$ are assumed constant. By combining Eqs. (2)–(5), the following expressions can be derived:

$$F^t = (e^* Aggr + \mu \bar{p} A) l_c b \tag{6}$$

$$F^n = \left(\frac{e^*}{\xi} Aggr + \bar{p} A \right) l_c b \tag{7}$$

To generalise the assessment even further and to gain a fundamental insight into the mechanics of wheel-workpiece interface laws, the stress relationships are derived for the grinding contact by normalising the forces with $l_c b$, thus removing the geometrical and kinematic effects of the process and focusing only on evaluating the wheel topography and workpiece:

$$\tau = e^* Aggr + \tau_0 \tag{8}$$

$$\sigma = \frac{e^*}{\xi} Aggr + \frac{\tau_0}{\mu} \tag{9}$$

where $\sigma = F^n/l_c b$ is the normal stress, $\tau = F^t/l_c b$ is the tangential stress, and $\tau_0 = \mu \bar{p} A$ is the sliding component of the tangential stress. The above stress variables have the units MPa while the intrinsic specific grinding energy has the units J/mm^3. Note that the two units are equivalent and are used interchangeably according to their corresponding physical context.

Although the expression for tangential stress (Eq. (8)) is equivalent to the grinding shear derived from the theory of aggressiveness [14], these are distinct equations. In the theory of aggressiveness, the grinding shear is derived from the general definition of total specific energy, $e = dP/dQ$, obtained from the grinding power and the material removal rate. Here, the specific energy depends on the process geometry and kinematics, which is bundled into the grinding aggressiveness, $Aggr$. In contrast, the intrinsic specific energy, e^*, is independent of grinding process parameters (e.g., depth of cut, wheel speed, workpiece speed), but captures the interaction between the grinding wheel topography and the workpiece material. In this respect, the above wheel-workpiece interface laws are complementing the theory of aggressiveness by focusing on workpiece and wheel effects.

2.2. Framework for evaluating wheel performance

The assessment framework focuses on quantifying how grit properties (toughness TI, thermal stability TS and aspect ratio AR) and dressing parameters (dressing aggressiveness $Aggr_D$) – along with their synergistic effects for a given bond type, workpiece material and cooling conditions – affect wheel topography. This is shown in Fig. 2.

The fundamental parameter used to quantify the geometric and kinematic effects of dressing is the dressing aggressiveness number, defined here as:

$$Aggr_D = \frac{1}{|1 - (\pm q)|} \sqrt{\frac{a_{ed}}{d_e U_d}} \tag{10}$$

where q is the dressing speed ratio ($q = v_r/v_s$), v_r is the dresser surface velocity, $U_d = a_{pd}/f_{ad}$ is the dressing overlap ratio, a_{pd} the active width of the dresser, f_{ad} is the diamond crossfeed velocity, a_{ed} is the depth of dress, and d_e is the equivalent wheel diameter. Here, the dressing
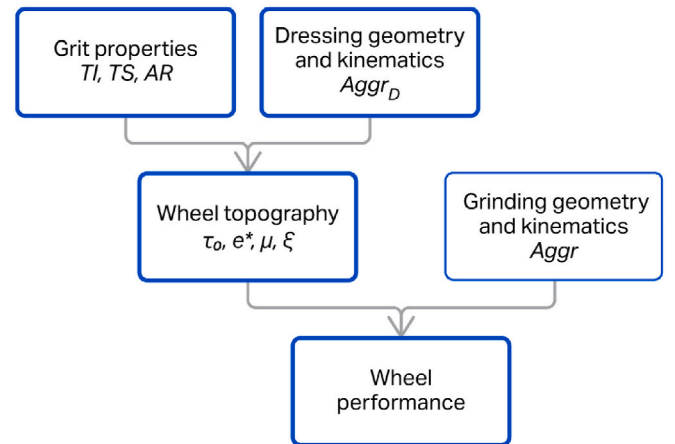
Fig. 2. Assessment framework. Wheel performance is affected by both the grinding process (quantified via $Aggr$) and wheel topography. It is measured by the newly introduced indicators τ_0, e^*, μ, and ξ. The wheel topography quantified with these indicators accounts for the synergistic effects between grit properties and dressing conditions (determined via $Aggr_D$).

aggressiveness number, $Aggr_D$, is simply the fundamental application of the dimensionless aggressiveness number, $Aggr$, with the dresser acting as the abrasive tool and the grinding wheel acting as the workpiece. It is worth mentioning that aggressiveness numbers are almost always significantly higher in dressing than in grinding. For example, $Aggr_D$ is in the order of 10^{-2}–10^{-3}, while $Aggr$ is in the order of 10^{-5}.

When dressing is performed in the unidirectional mode (i.e., q is positive number) with similar surface speeds for the grinding wheel and dressing tool, the speed ratio approaches unity ($q = +1.0$), resulting in significantly higher values of aggressiveness. At the extreme condition of $q = +1.0$, the aggressiveness approaches infinity, $Aggr_D \to \infty$. In such a case there is no relative tangential movement ($v_s - v_r = 0$), only normal motion, which causes grit crushing. Since relative tangential movement is a characteristic of all abrasive interactions, including dressing, the majority of dressing processes are not operated at the extreme condition ($q = +1$). If the speed ratio is indeed unity ($q = +1.0$), the process is quite different, with different contact and removal mechanisms, and is referred to as "crush dressing" [22].

A schematic illustration of grinding-response assessments is shown in Fig. 3a. While the characteristic total specific energy curve is the most common indicator of grinding efficiency for a given wheel-workpiece combination and a given set of dressing and cooling conditions, it does not directly link with wheel topography. In addition, it is challenging to distinguish between the energy associated with cutting and the energy associated with rubbing and ploughing. On the other hand, the proposed performance assessment (Fig. 3b) is capable of quantifying and evaluating the topography effects via the four performance indicators included in the wheel-workpiece interface laws: e^*, τ_0, μ and ξ. The parameter e^* can be extracted from the slope of the $Aggr-\tau$ curve and the parameter τ_0 can be extracted from the intercept. Considering also the normal stress σ, additional parameters ξ and μ can be obtained. The latter, μ, is a ratio of the intercepts of the linear regression applied to the pairs $(Aggr, \tau)$ and $(Aggr, \sigma)$.

The proposed parameters (e^*, τ_0, ξ and μ) are hence useful quantitative indicators of the wheel performance over a range of grinding conditions for an arbitrary $Aggr$, i.e. a given set process geometry and kinematics.

The proposed framework for wheel-performance assessment does not consider the progression of grinding wheel wear. It assumes that, for a given workpiece and wheel topography, the wear flat area (A_{sl}) is constant. The reason for this is that cBN wheels wear significantly slower than conventional-abrasive wheels [23]. In addition, the objective of the test method is to evaluate the grinding wheel performance after dressing without prolonging the test to account for the wheel wear.

3. Grit and grinding-wheel characterisation

3.1. Grit properties TI, TS and AR

The focus of this study is to evaluate the effect of the grit properties – specifically toughness (TI), thermal stability (TS) and aspect ratio (AR) – on the grinding process. Therefore, it is essential to clarify how these distinct grit properties are determined. Note that while the focus of this investigation is on cBN grits, the framework, as well as majority of characterisation techniques, is not limited to any specific grit type.

Two key mechanical properties of cBN grits are the toughness index (TI) and the thermal stability (TS). The TI measures a grit's resistance to fracture. It is an arbitrary measure of the breakdown resistance of the abrasive under impact loading. A high TI signifies a low percentage breakdown of grits. Thermal stability is the grit's ability to maintain its properties (hardness, toughness, resistance to oxidation and chemical breakdown, etc.) at elevated temperatures. Despite the availability of an international standard [24], grit-manufacturers tend to develop their own proprietary techniques for evaluating mechanical properties. The mentioned international standard quantifies the toughness by measuring the time at which approximately 50% of starting material is left on a defined sieve after oscillatory motion of the precision capsule containing grit and a steel ball [24]. In this study, a toughness measurement was made of the weight of abrasive retained on a defined sieve at a set time after using the same test principle (see Fig. 4). Thermal stability is measured in the same manner but after exposing the grit to elevated temperatures (1100 °C). In this case thermal stability defines changes in toughness after being exposed to high temperature which is relevant for wheel making process [25]. In this process the temperatures can reach high enough levels to further reduce the toughness of the grit that has low thermal stability.

Both the TI and TS properties determine how well a grinding wheel can resist wear and, consequently, retain its surface topography. Broadly speaking, grits with higher values of TI and TS last longer, while weaker grits (lower values of TI and TS) break down faster, resulting in a shorter tool life (lower G-ratio) [26]. Consequently, wheels with low values of TI and TS typically (but not always) require more frequent dressing. However, wheels containing grits with low TI can have the benefit of being "self sharpening", meaning dull grits fracture to expose new, sharp cutting edges.

The primary geometrical features of grits are size and shape. According to international standards, grit size is determined through sieving [27,28]. In this investigation, grit size (c) is analysed with the Camsizer® XT device. The grit shape, characterised by its average aspect
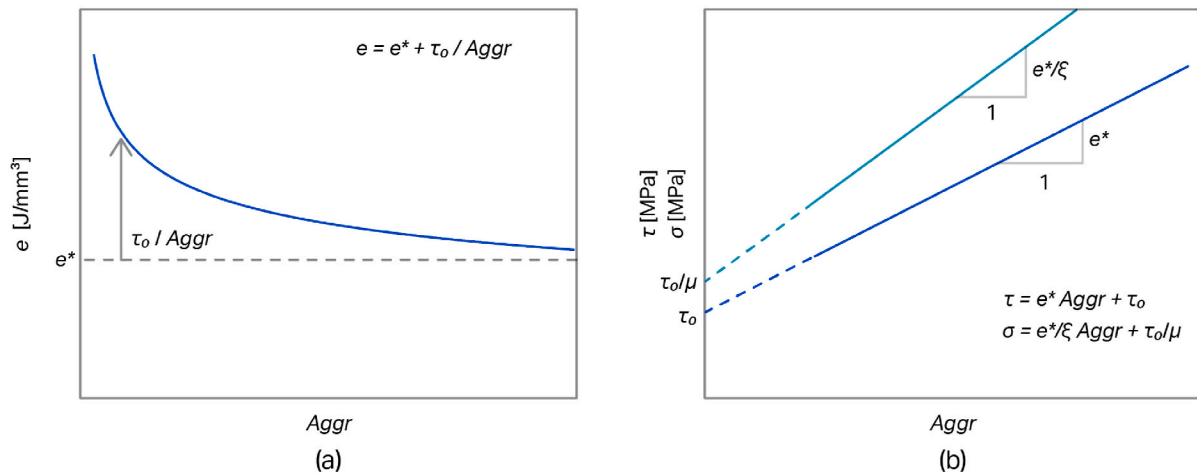
Fig. 3. Wheel-performance indicators vs. grinding aggressiveness. The graphs are plotted as: a) the characteristic specific energy curve [14]; and b) the grinding response in $(Aggr, \tau)$ and $(Aggr, \sigma)$ diagrams, where the introduced performance indicators can be easily obtained (e^*, τ_0, ξ and μ). Note that the illustrations are general, i.e., not based on actual measurements.
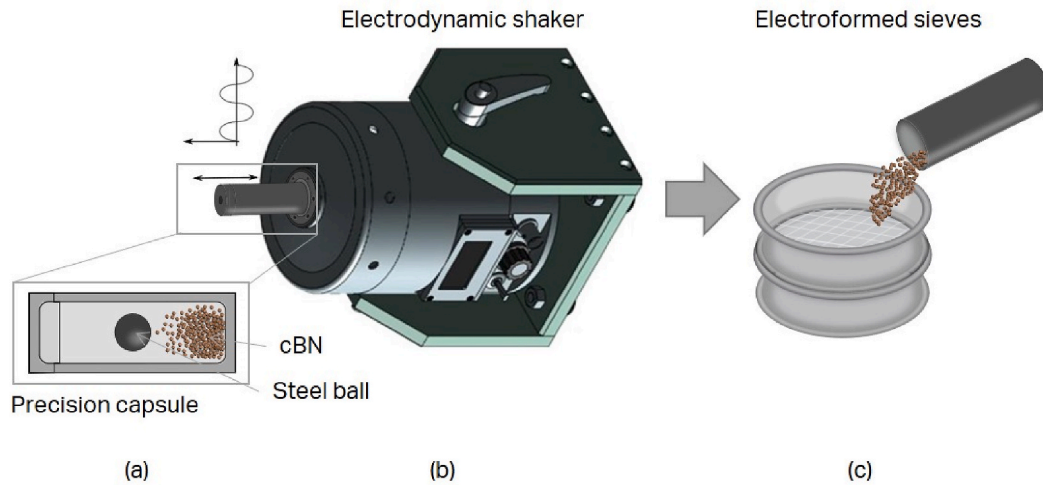
Fig. 4. Friability test used to measure toughness of grits and thermal stability of grit that has been exposed to 1100°C). (a) A steel ball and a specified amount of grits are placed into a precision capsule which is mounted to (b) an electrodynamic shaker, which is run for a set amount of time, during which the grits are crushed by the steel ball; (c) fractured material is then sieved and grits left on the defined sieve are weighed and compared to the weight of the original material. A tougher grit will retain more of the material in its original size range.

ratio (*AR*), is captured from 2D-image projections as schematically shown in Fig. 5. The aspect ratio is defined as the ratio between the shortest cord and longest Feret diameter of grits in 2D projections.

3.2. Grinding-wheel topography

Vitrified-bonded grinding wheels are challenging to image due to their inherent porosity. To overcome the variation of the grit protrusion and the depth-of-field issue, an image-stacking technique was used to obtain 3D images using a Keyence VH500 digital microscope. Images were taken at 150X magnification, yielding an evaluation area of 1.8 mm × 2.4 mm with a stacking height of 5 μm. Several equally distanced images were taken around the periphery of the grinding wheel at the end of grinding runs. These images were then overlaid with height maps followed by a colour-threshold analysis using Image-J processing software. This enabled the evaluation of the average percent of wear-flat area (*A*) (Fig. 6a), which is considered constant throughout the test. While grit-protrusion height can be easily measured on electroplated wheels using optical microscopy, it is more challenging with vitrified-

bonded wheels. Therefore, an alternative approach was introduced where the percent of contact area (α) was estimated at different wheel depths, as shown in Fig. 6b. The rate of increase of α, $\Delta\alpha$, indicated the average grit protrusion – i.e., the larger the $\Delta\alpha$ value, the lower the protrusion of grits at the wheel surface.

4. Grinding experiments

Grinding tests were carried out using a Blohm MT408 surface grinding machine. The workpiece material was 100Cr6 (AISI/SAE 52100) through-hardened bearing steel with a hardness of 60-61HRC. Forces were measured with a two-component Kistler 9257A dynamometer. The grinding fluid was Hocut 768 water-based emulsion (4.5–5.0% concentration) delivered to the grinding zone at 9 bar. A 40-bar high-pressure cleaning nozzle was used to remove residue from the grinding-wheel pores.

To measure small differences in wheel topography, a specific test, called window-of-operation (see Fig. 7), was used to evaluate the grinding wheels under two sets of dressing parameters by changing f_{ad},
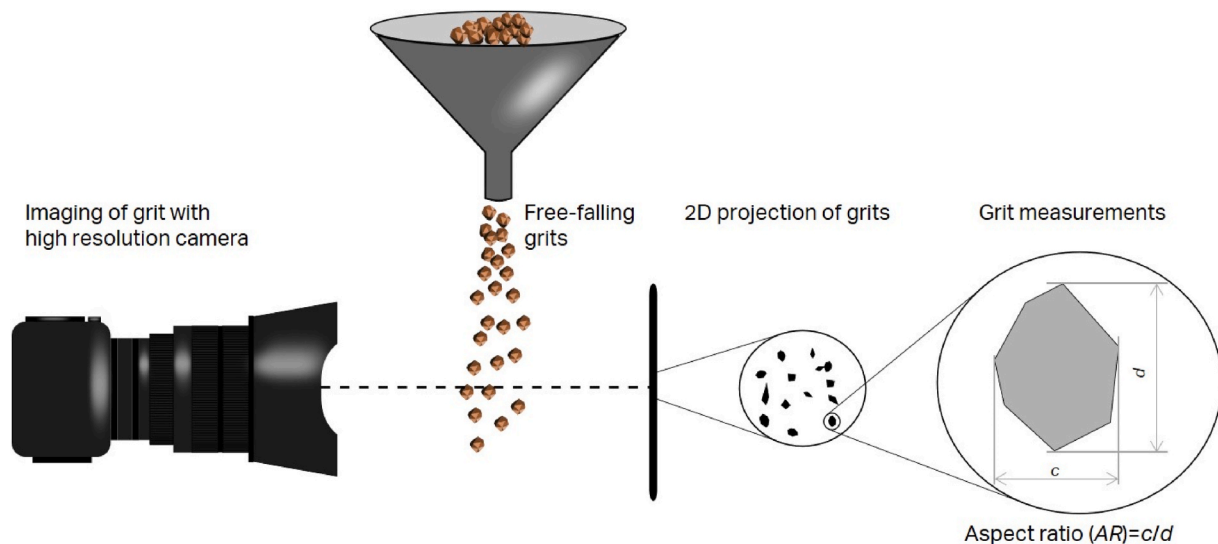
Fig. 5. Schematic illustration of average aspect ratio (*AR*) estimation for grits (adapted from Ref. [29]). $AR = c/d$ is based on the shortest chord *c* (generally equivalent to sieving) and the longest Feret diameter *d* obtained from a 2D projected image of a grit. The shortest cord *c* is also used to express the size of the grit.
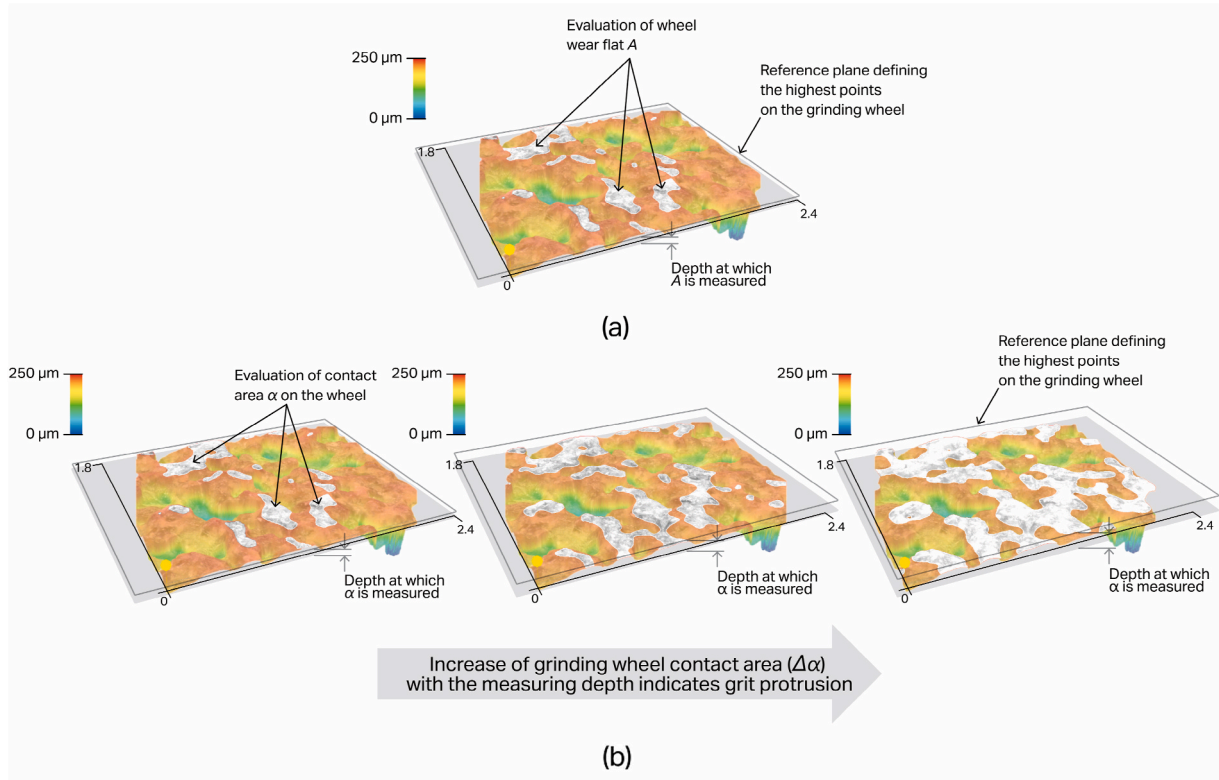
Fig. 6. Wheel topography analysis after dressing. a) Wheel wear-flat area A is analysed by measuring the amount of highlighted white area on the topmost layer of the grinding wheel and is considered constant; b) the grit protrusion $\Delta\alpha$ is evaluated incrementally by measuring the increase of α (indicated by the highlighted white area) with grinding wheel depth.
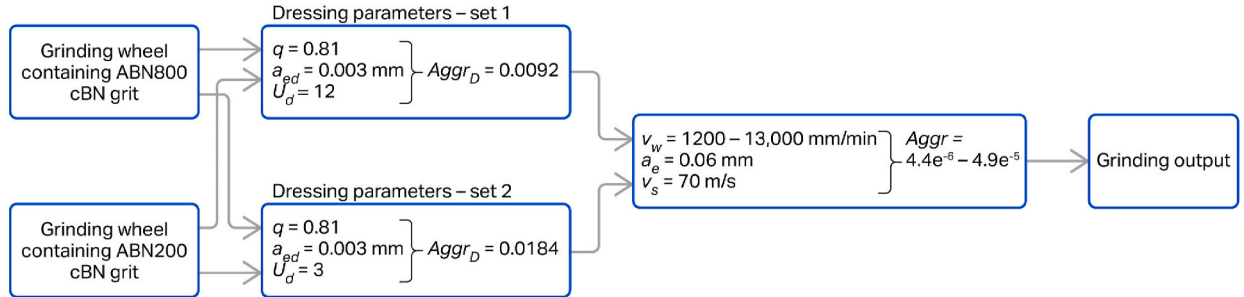
Fig. 7. Design of experiments. Two grinding wheels, one with ABN200 and one with ABN800 cBN grits, are dressed with two sets of dressing parameters ($Aggr_D = 0.0184$ and $Aggr_D = 0.0092$). Dressing is followed by a set of grinding trials over a wide range of grinding process parameters (ranging from $Aggr = 4.4\mathrm{e}^{-6}$ to $4.9\mathrm{e}^{-5}$). The grinding output is analysed using the developed framework for evaluating wheel performance.

yielding different values of U_d: the first with $Aggr_D = 0.0184$ (sharp dress), the second with and $Aggr_D = 0.0092$ (dull dress). The dressing tool was a rotary dresser with a single layer of vertically plated diamond grits (FEPA D426). Each new set of dressing parameters was followed by 15 grinding passes to reach steady wheel behaviour after the initial transitional period after dressing, as shown by Ref. [15]. The purpose was to evaluate the wheels over a wide range of $Aggr$ values by changing v_w while keeping a_e and v_s constant (see Fig. 7). After each change in v_w (and therefore $Aggr$), only three passes were made to ensure negligible wear and maintain the wheel topography that was established for the respective variations in grit properties and dressing conditions.

All grinding tests were carried out with vitrified-bonded grinding wheels with b151-size cBN grits with a concentration of 6.6 ct/cm³ (C150).

5. Results and discussion

5.1. Grit characterisation

Two monocrystalline grades of cBN were considered in the study: ABN200 and ABN800 (Fig. 8). ABN200 is black, with low toughness and low thermal stability. ABN800 is brown, with high toughness and high thermal stability. The toughness results of both were obtained from three samples. The normalized results are shown in Fig. 9. ABN800 is approximately 30% tougher and 60% more thermally stable than ABN200. In other words, ABN800 is more resistant to fracture and less susceptible to thermal degradation compared to ABN200.

The distributions of measured grit size (c) and aspect ratio (AR) are shown in Fig. 10. Three samples of each grit type were evaluated. In practise, distributions are often compared through three points obtained from a cumulative distribution function; D10, D50 and D90. These
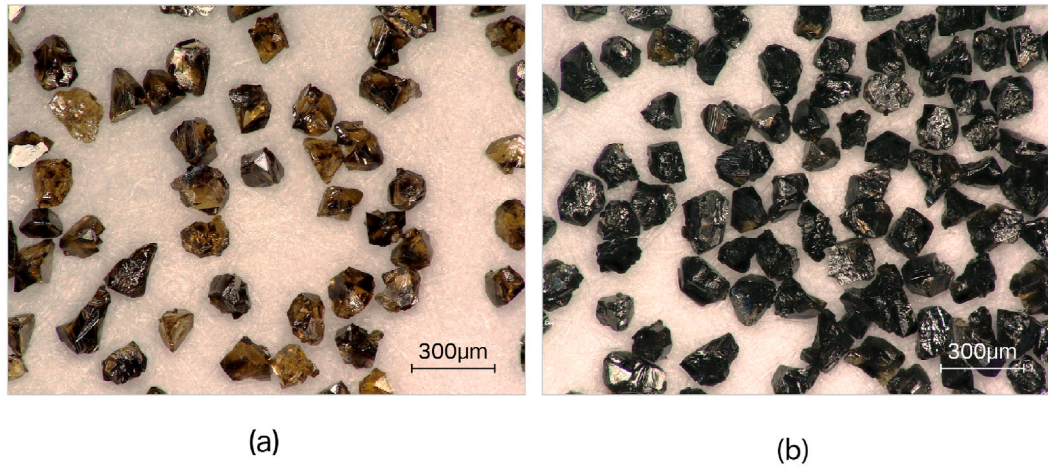
Fig. 8. The two types of cBN grits used in experiments. a) ABN800 is a brown grit with higher toughness and higher thermal stability; b) ABN200 is a black grit with lower toughness (i.e., a more friable grit) and lower thermal stability. (For interpretation of the references to colour in this figure legend, the reader is referred to the Web version of this article.)
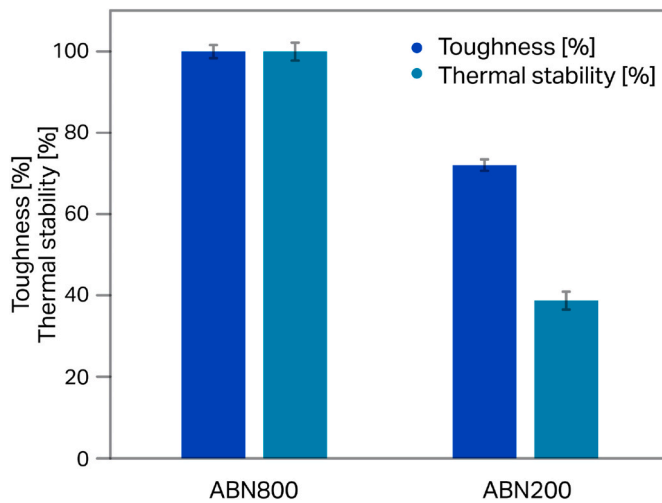
Fig. 9. Toughness and thermal stability of ABN800 and ABN200. The values have been normalized against ABN800. The error bars represent the standard deviation.

represent the volume of grits for the size and shape below 10%, 50% and 90%. The median values for c and AR (i.e. D50) are given in Table 1.

The differences detected between the two grades can be considered minimal, i.e. approximately Δ 4% in c and Δ 2.5% in AR. As it is evident from mechanical and geometrical grit measurements that the most notable properties differences between ABN800 and ABN200 are toughness (TI) and thermal stability (TS).

5.2. Grinding response when evaluating wheel performance

The key objective of the experimental investigation is to evaluate the effects of grit properties and dressing on performance indicators. Results obtained when grinding with wheels containing ABN800 and ABN200

Table 1
D50 values for ABN800 and ABN200. Measurements represent the median for grit size (c) and shape-aspect ratio (AR). Values are recorded as the average of three median values of three measured samples ± SD of the three average values.

Grit type	c [μm]	AR
ABN800	146 ± 2.1	0.711 ± 0.016
ABN200	152 ± 4.2	0.728 ± 0.007
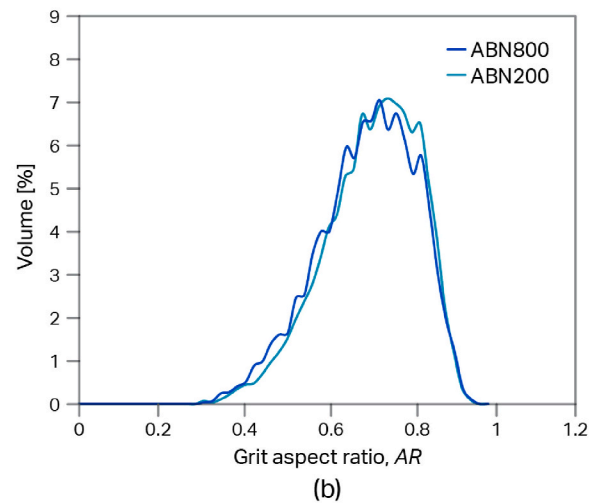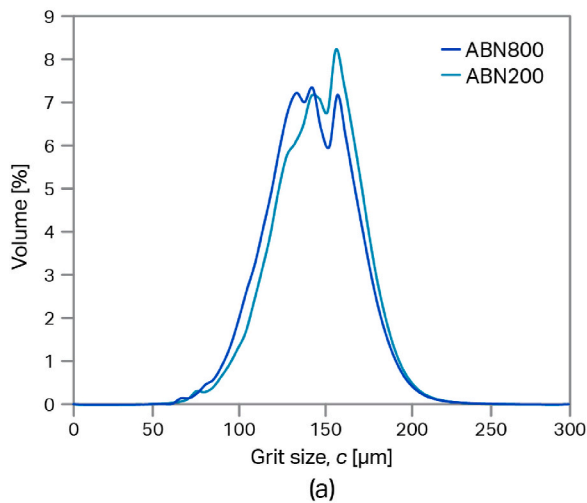
Fig. 10. Distributions of geometrical features of ABN800 and ABN200. a) grit size c expressed as the shortest cord (generally equivalent to sieving); and b) aspect ratio AR. Values are recorded as the average of the three measurements.

grits (with $Aggr_D = 0.0092$) are shown in Fig. 11. We can divide the graph into two distinct regimes. The first regime, at low *Aggr*, can be attributed to process that is dominated by ploughing, rubbing and nonconforming contact between wheel topography and the workpiece surface as proposed by Malkin and Cook [2]. In this regime, τ and σ increase faster for each increment of *Aggr* compared to the second regime. In the second regime ($Aggr \geq Aggr_0$), the wheel and the workpiece are fully engaged (i.e., contact between the wheel and the workpiece is conforming) and cutting dominates as the contact mechanism. In this regime there is a linear relationship between the τ and *Aggr* as well as σ and *Aggr*. Although the grinding power (P) and specific material removal rate (Q') plots can provide similar trends – as reported by Refs. [15,17] – the two regimes are less pronounced and can be even unidentifiable due to the characteristic nature of Q' when compared to *Aggr*. The results also suggest that the transition from the first regime to the second is similar for both grit types at lower $Aggr_D$, suggesting that the grit properties (i.e. *TI* and *TS*) do not affect the transition significantly. Normally, the transition range is easier to identify in the $\sigma - Aggr$ diagram since $\sigma > \tau$.

The developed assessment framework is primarily intended to analyse regime II, i.e. beyond the transition aggressiveness number ($Aggr_0$) where the relationship between grinding input and output is linear.

Fig. 12 shows the results from the sharper dressing ($Aggr_D = 0.0184$). Here, there is no clear distinction between the two grinding regimes. This suggests that the dressing conditions have a dominant effect on the wheel topography and, consequently, grinding response. This was also observed by Shaw [30] who found that low values for U_d (and, consequently, high values for $Aggr_D$) lead to a larger chip thickness and a more efficient grinding process dominated by cutting. This suggests that the transition from regime I to regime II lies at values of *Aggr* lower than those tested here.

A linear fit applied to regime II for the two plots ($Aggr, \tau$ and $Aggr, \sigma$) was used to extract the performance indicators for ABN200 and ABN800 dressed with different values of $Aggr_D$. They are summarised in Table 2.

In the case of ABN800 grits, the intrinsic specific grinding energy e^* is 32% higher for the dull-dressed wheel ($Aggr_D = 0.0092$) compared to the sharp-dressed wheel ($Aggr_D = 0.0184$). The higher dressing aggressiveness causes more grit fragmentation and a sharper wheel, resulting in less rubbing and ploughing. The change in intrinsic specific grinding energy e^* due to dressing indicates that there is an additional energy dissipated at the interface that is proportional to *Aggr*. Moreover, this extra sliding energy is more pronounced for ABN200 wheels with

the smaller $Aggr_D$. Similar to intrinsic specific grinding energy e^*, the sliding component of tangential stress τ_0 is about 55% higher for the dull-dressed ($Aggr_D = 0.0092$) ABN800 wheel, suggesting that wear flat area A is more pronounced at lower $Aggr_D$. To generalise, finer dressing with lower $Aggr_D$ will result in a larger initial wear flat area on the wheel. Interestingly, the friction coefficient μ and the cutting force ratio ξ appear to be unaffected by the dressing conditions.

The trends observed above for ABN800 can be extended to ABN200. The intrinsic specific grinding energy e^* increases when the wheel is dressed dull with low $Aggr_D$ (see Table 2). Moreover, e^* values for ABN200 are larger compared to ABN800 for the same dressing conditions. These results suggest again that there is an additional dissipation of energy at the wheel-workpiece interface proportional to *Aggr*. However, the increase of intrinsic specific grinding energy e^* cannot be contributed solely to changes of dressing conditions, but also to the grit properties (i.e. *TI* and *TS*). This is reflected in distinct values for e^* for the same dressing conditions. In the case of sliding component of tangential stress τ_0, there is a notable increase (about 88%) for the dull dress ($Aggr_D = 0.0092$), as percent of wheel wear flat area A increases with lower $Aggr_D$ values. In addition, it appears that more wear flats A are generated on the wheel surface, as ABN200 has lower *TI* and *TS* values compared to ABN800 grit. The slope of the grinding force ξ is similar to ABN800, but μ is considerably larger for $Aggr_D = 0.0092$. The differing values for μ imply extra rubbing at the interface that can be attributed to bond-workpiece.

To further understand the contact between the wear flats and workpiece, the wheel topography was evaluated as described in Section 3.2. The topography analysis of the ABN200 and ABN800 wheels reveals that, overall, the wheel wear flat area A, is lower for sharply dressed wheels (Fig. 13a), which is to be expected. This indicates that sliding component of tangential stress τ_0 is indeed a representation of grit wear flat area A. Additionally, ABN200 has a consistently higher portion of percent wheel wear flat area A compared to ABN800 when dressed with the same conditions. The likely reason is that the toughness of the grit affects the likelihood of grit fracture (as opposed to bond fracture) during dressing. Hence, wheels containing grits with low *TI* are more likely to generate more wear flat area at the surface due to micro-chipping of the grits. Low *TS*, in this case, can further reduce toughness due to potential exposure to high temperature during wheel manufacturing and for that reason it can also contribute to wear flat generation. In contrast, stronger grits (higher *TI* and *TS* values) are more likely to macro-chip (or fracture out of the bond material) and generate sharper cutting edges, resulting in a lower wheel wear-flat area A. Images of the ABN800 and ABN200 wheels at a depth of 10 μ m from the
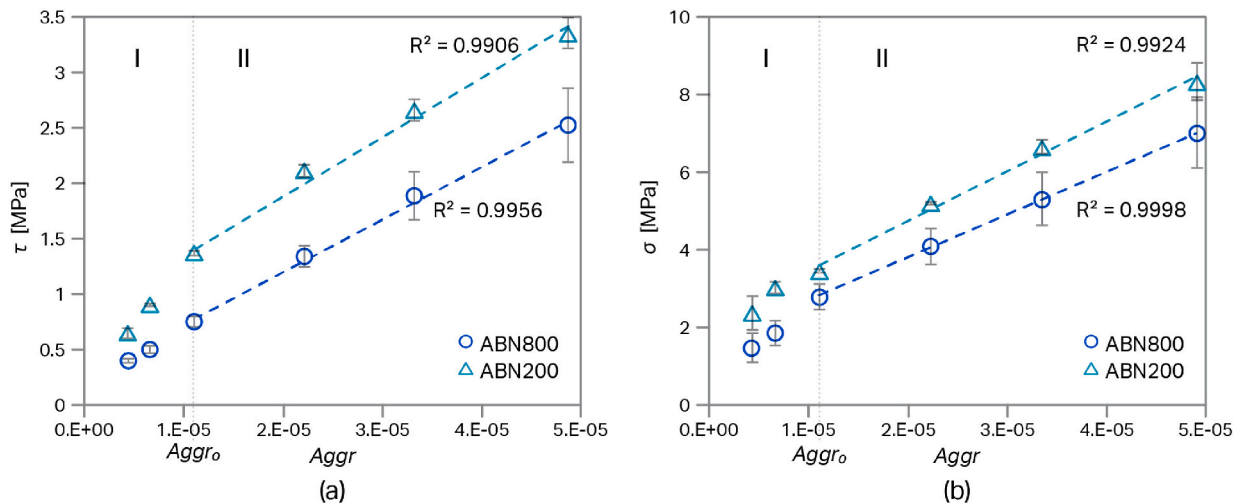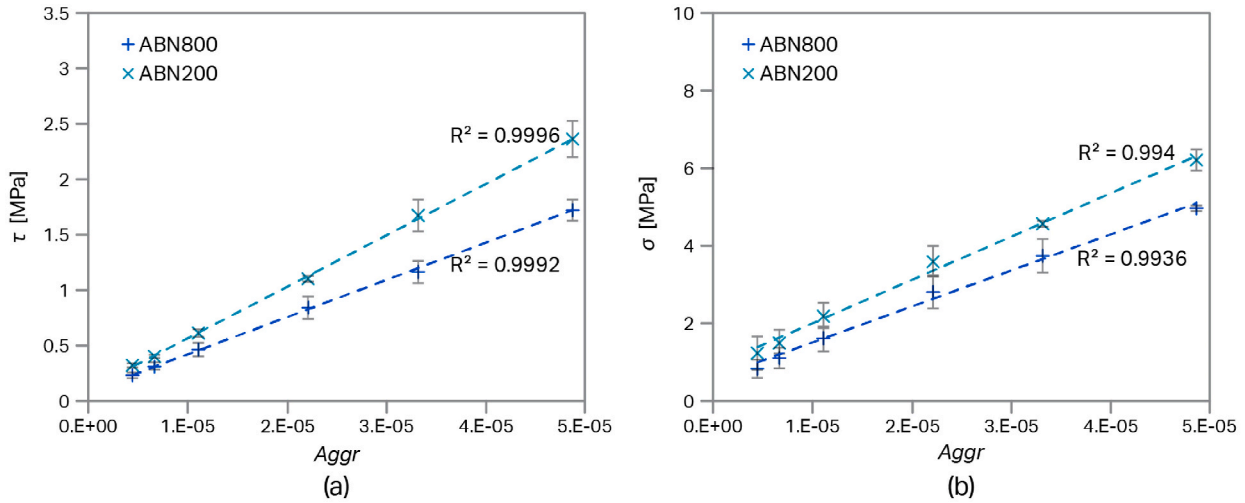

Fig. 11. Grinding results when wheels are dressed with $Aggr_D = 0.0092$ (i.e. dull dress). The difference in grinding performance for ABN800 and ABN200 wheels: a) $Aggr - \tau$ and b) $Aggr - \sigma$ plots from where the performance indicators e^*, τ_0, ξ and μ can be extracted. The error bars represent the standard deviation.

Fig. 12. Grinding response when wheels are dressed with $Aggr_D$ =0.0184 (i.e. sharp dress). The difference in grinding performance between ABN800 and ABN200 wheels: a) $Aggr - \tau$ and b) $Aggr - \sigma$ plots from where the performance indicators e^*, τ_0, ξ and μ can be extracted. The error bars represent the standard deviation.

Table 2
Performance indicators (e^*, τ_0, ξ and μ) for ABN800 and ABN200 grits, extracted from the $Aggr - \tau$ and $Aggr - \sigma$ plots.

Grit type	$Aggr_D$	e^* [J/mm^3]	τ_0 [MPa]	ξ	μ
ABN800	0.0092	48.6	0.212	0.39	0.18
ABN800	0.0184	33.2	0.095	0.36	0.17
ABN200	0.0092	52.2	0.882	0.41	0.39
ABN200	0.0184	46.5	0.103	0.42	0.12

wheel outer surface for the two different dressing conditions are illustrated in Fig. 13b, where the white highlighted area represents the grit wear-flat area.

Dressing parameters and grit properties appear to affect the intrinsic specific energy due to the extra rubbing and ploughing likely caused by (i) the vitrified bond surface that is in contact with the workpiece and (ii) debris formed during the chip formation. A simple way to investigate the additional energy observed in e^* is to evaluate the average grit protrusion $\Delta\alpha$ or the variation of the contact areas with respect to depth

(as described in Section 3.2). An estimate of the average grit protrusion $\Delta\alpha$ – for both wheels and for both aggressiveness values – is shown in Fig. 14a. An illustration of how the protrusion is estimated is shown in Fig. 14b. Note that the average grit protrusion for both of the wheels is larger (lower $\Delta\alpha$) for sharply dressed wheels ($Aggr_D = 0.0184$) suggesting that the dresser not only affects the wear flat area, but also the protrusion of the abrasive grits. In addition, the grit protrusion is lower for the ABN200 wheel for both dressing conditions, indicating that TI and TS also affect the grit projection at the wheel surface. The obtained correlation between intrinsic specific grinding energy e^* and the average grit protrusion $\Delta\alpha$ indicates that the additional energy dissipated at the interface is associated with a rubbing process due to grit protrusion.

To further illustrate the application of the assessment framework, an additional grinding data set (published by Macerol et al. [17]) was analysed. The data featured two distinct grit shapes: $AR = 0.78$ ('blockier') vs. $AR = 0.54$ ('elongated'), both with comparable grit size (b126) and TI and TS properties. All tests were conducted with the wheels dressed at identical conditions ($Aggr_D = 0.0156$). The results are shown in Fig. 15. A summary of the $Aggr - \tau$ and $Aggr - \sigma$ plots are given
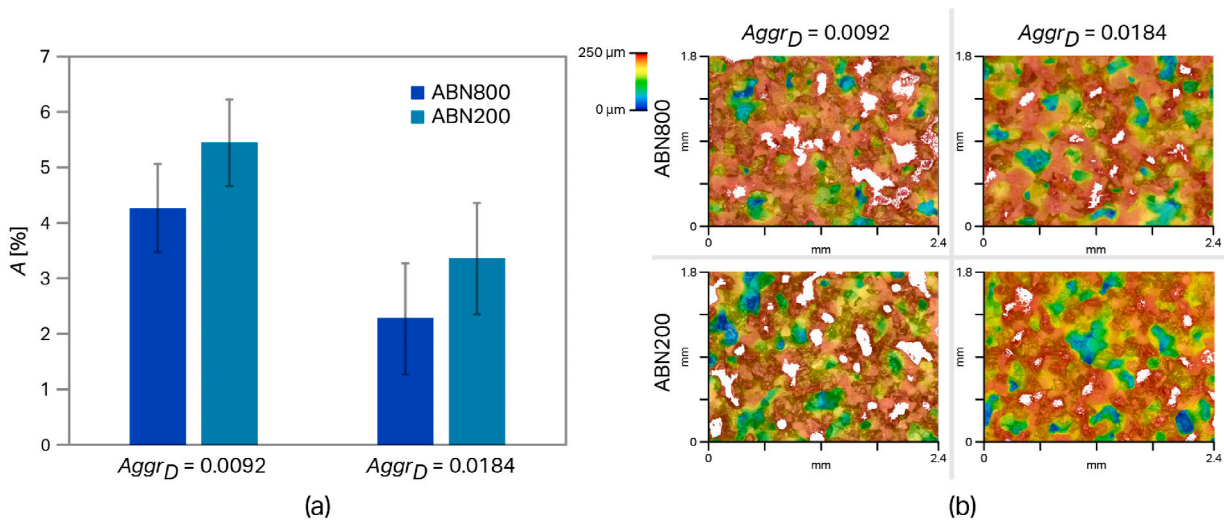
Fig. 13. Analysis of the percent of wear flat area A for ABN800 (tougher) and ABN200 (more friable) grinding wheels after dressing. a) Values for wear-flat area A for both wheels, dressed dull ($Aggr_D = 0.0092$) and sharp ($Aggr_D = 0.0184$) and b) processed surface images of both wheels, with wear flat-area shown in white.
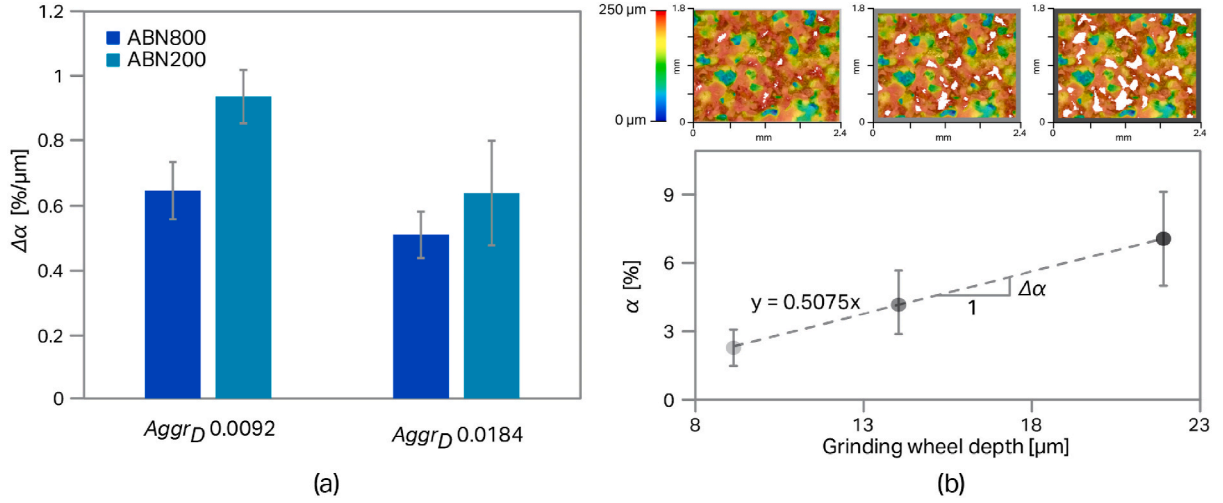
Fig. 14. Average grit protrusion. a) $\Delta\alpha$ for ABN800 and ABN200 wheels dressed at $Aggr_D = 0.0184$ and $Aggr_D = 0.0092$; the higher $\Delta\alpha$ indicates less protrusion and vice versa (error bars represent the standard deviation); b) an example of the average grit protrusion estimate for the ABN800 wheel (with $Aggr_D = 0.0184$) by measuring wheel-contact area α increase with a higher grinding wheel depth.

in Table 3. The results suggest that intrinsic specific grinding energy e^* is unaffected by AR. In contrast, the sliding component of tangential stress, τ_0, changes with AR (Table 3). Here, the blockier grit (higher AR) yields higher τ_0 while the opposite trend is observed when using the elongated grit (lower AR). These findings strongly suggest that grit shape has a pronounced effect on the wheel wear flat area A and, consequently, on τ_0. Also, the cutting efficiency, which is indicated by the intrinsic specific grinding energy e^* value, is independent of the grit shape. Considering this, it may not be necessary to expand the wheel-topography assessment and modelling to account for grit angles [31] for the case of grinding with vitrified cBN grinding wheels.

The application of the proposed assessment framework for evaluating wheel performance highlights the importance of considering grit properties and their effects on grinding. Therefore, the geometry and physical properties of grits should be considered in the grinding analyses. For example, the results showed that the same dressing conditions on wheels with distinct grit properties generate very different wheel topographies and, consequently, result in different grinding responses. In the case study presented here, the ABN800 wheel, with the higher *TI* and *TS* compared to the ABN200 wheel, yielded a lower intrinsic specific

Table 3

Performance indicators for grits with different aspect ratio, *AR*. The values are extracted from the $\tau - Aggr$ plot in Fig. 15.

AR	e^* [J/mm^3]	τ_0 [MPa]
0.78	44.3	0.567
0.54	43.0	0.180

grinding energy e^* both when dressed sharp ($Aggr_D = 0.0184$) and dull ($Aggr_D = 0.0092$), as shown in see Fig. 16. At the same time, the ABN800 wheel exhibited a much smaller value of sliding component of tangential stress τ_0 when dressed dull but approximately the same value of τ_0 when dressed sharp. In the case of the ABN200 wheel, the additional contact at the interface is responsible for a relative increase in intrinsic specific grinding energy e^*, sliding component of tangential stress τ_0 and friction coefficient μ (for $Aggr_D = 0.0092$). This is likely caused by an increase in wear-flat area A and a decrease in the average grit protrusion $\Delta\alpha$ as a result of the lower values for *TI*. Grits with lower *TS* can potentially act similarly, because their toughness can reduce if they are exposed to higher temperatures, which can happen during wheel manufacturing.
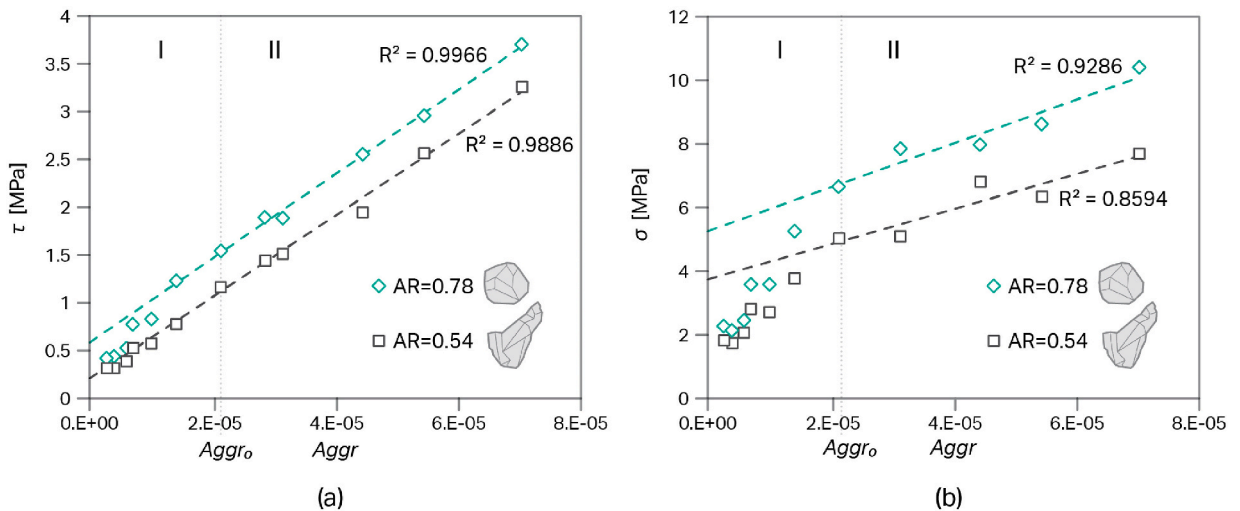
Fig. 15. Results when grinding with wheels of comparable grit size (b126), *TI* and *TS*, but with different grit shapes: blocky ($AR = 0.78$) vs. elongated ($AR = 0.54$) under the same dressing conditions ($Aggr_D = 0.0156$). a) $Aggr - \tau$ and b) $Aggr - \sigma$ plots. The error bars represent the standard deviation. Data was adapted from Ref. [17].
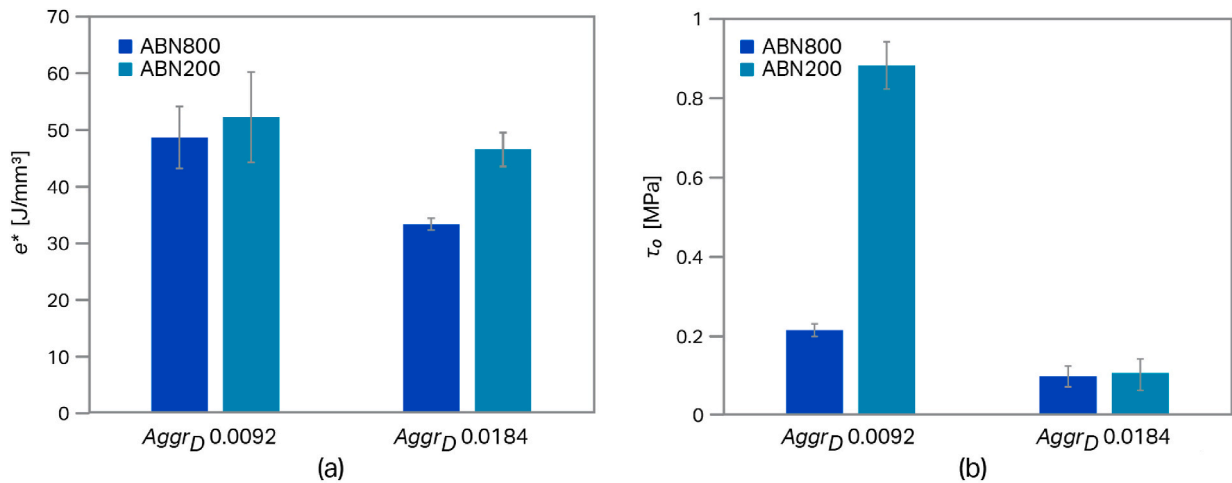
Fig. 16. Performance indicators for different grit types and dressing conditions. a) The intrinsic specific grinding energy (e^*); and b) the sliding component of tangential stress (τ_0) for ABN200 and ABN800 cBN grits for two distinct dressing conditions (sharp and dull). The error bars represent the minimum and maximum values.

Additionally, grits with a high *TI* and *TS* (ABN800) retain better sharpness across a wider range of grinding *Aggr* and dressing $Aggr_D$ conditions, whereas the weaker grits (ABN200) are characterised by a higher wear-flat area regardless of the dressing conditions. Moreover, the wear flat area on the wheel surface controls the size of regime II and, thus, the window of grinding operating conditions. It is well known that smaller values for $Aggr_D$ lead to improved surface finish; nevertheless, the additional contact at the interface can causes an increase in rubbing and, consequently, higher heat generation during grinding.

Based on the presented case studies, it is possible to generalise the findings with regard to grinding responses based on grit properties (*TI* and *TS*) and dressing conditions ($Aggr_D$), as shown in Fig. 17. The characteristic grinding responses are schematically illustrated in the $Aggr - \tau$ and $Aggr - e$ plots. Additionally, the characteristics of the wheel topography are exemplified for different values of percent wear-flat area *A* and grit protrusion $\Delta\alpha$. Therefore, the effect of wheel-workpiece interaction can be captured using the approach presented here.

6. Conclusions

The primary aim of this paper was to develop an analytical framework for evaluating grinding wheel performance that can account for the effects of grit properties and dressing conditions on the wheel topography and, in turn, grinding performance. Such information is normally not available when using more established grinding-performance measures such as the characteristic specific grinding energy curve plotted against aggressiveness number, which fully accounts for process geometry and kinematics but does not explicitly consider surface-topography effects. Based on the classical Malkin and Cook model [2,3], where the wear flat-area developed on the grits uniquely determines the grinding-force components for a particular workpiece material and grinding conditions, a new set of new performance indicators are derived and then used to evaluate the effect of the wheel topography on the grinding process. The framework is applicable to a grinding regime that is dominated by cutting, with limited portions of rubbing and ploughing. In such a regime, which requires a certain (threshold) aggressiveness, a plot of τ versus *Aggr* should yield a straight line whose slope is proportional to intrinsic specific grinding energy e^*, meaning that the correlation between tangential and normal stress is linear. It is further demonstrated that e^* is sensitive enough to distinguish between different grit protrusions, while sliding component of tangential stress τ_0 fundamentally captures the percent of wheel wear-flat area. Additional contact between the wheel and the workpiece when grinding with a dull wheel is further captured via the friction

coefficient μ and the cutting efficiency with the force inclination. The grit best suited for a particular workpiece should have both a low attritious wear rate and a low rubbing friction coefficient.

The proposed framework is experimentally verified and demonstrated via grinding tests using wheels with different grit types and dressing conditions, as this makes it possible to distinguish between characteristic wheel topographies. An underlying theoretical basis for this evaluation can be seen by deriving and plotting the relationships between the tangential and normal stresses at the wheel-workpiece interface vs. the grinding aggressiveness. At a fixed grinding aggressiveness, both process geometry and kinematics remain constant. However, the observed differences in grinding responses can be associated with grit properties and/or dressing conditions, both of which affect wheel topography. Results show that the intrinsic specific grinding energy e^* increases when wheels are dressed "duller", i.e. with a lower dressing aggressiveness. The different values for e^* indicate that the energy dissipated at the interface is also proportional to additional rubbing. When the wheels are dressed "sharp", the window of operating grinding conditions is wider. The sliding component of tangential stress τ_0 is proportional to the grit wear-flat area generated during dressing. Grits with different aspect ratios *AR* produce different amounts of wear-flat area during dressing, whereas the grit toughness *TI* and grit thermal stability *TS* affect the wear-flat area and the overall grit protrusion, which is usually not considered in the grinding analysis. Other specific conclusions resulting from experimental work are summarised as follows:

- ABN800 grit produces a lower intrinsic specific grinding energy e^* and lower sliding component of tangential stress τ_0 due to its high toughness *TI*. High thermal stability *TS* likely contributes to the result considering that the toughness is less likely to be affected when exposed to higher temperatures, which can occur during the wheel making process.
- The transition from rubbing/ploughing to cutting is more pronounced for wheels dressed duller (lower $Aggr_D$). The transition appears unaffected by grit properties (*TI*, *TS* and *AR*).
- The results indicate that a) the sliding component of tangential stress τ_0 is primarily affected by the wear-flat area *A* and b) the intrinsic specific grinding energy e^* is primarily affected by the grit protrusion $\Delta\alpha$. As a result, both increase if the wheel is dressed duller (lower $Aggr_D$).
- The friction coefficient μ depends on a combination of different rubbing actions at the interface and is affected by dressing conditions
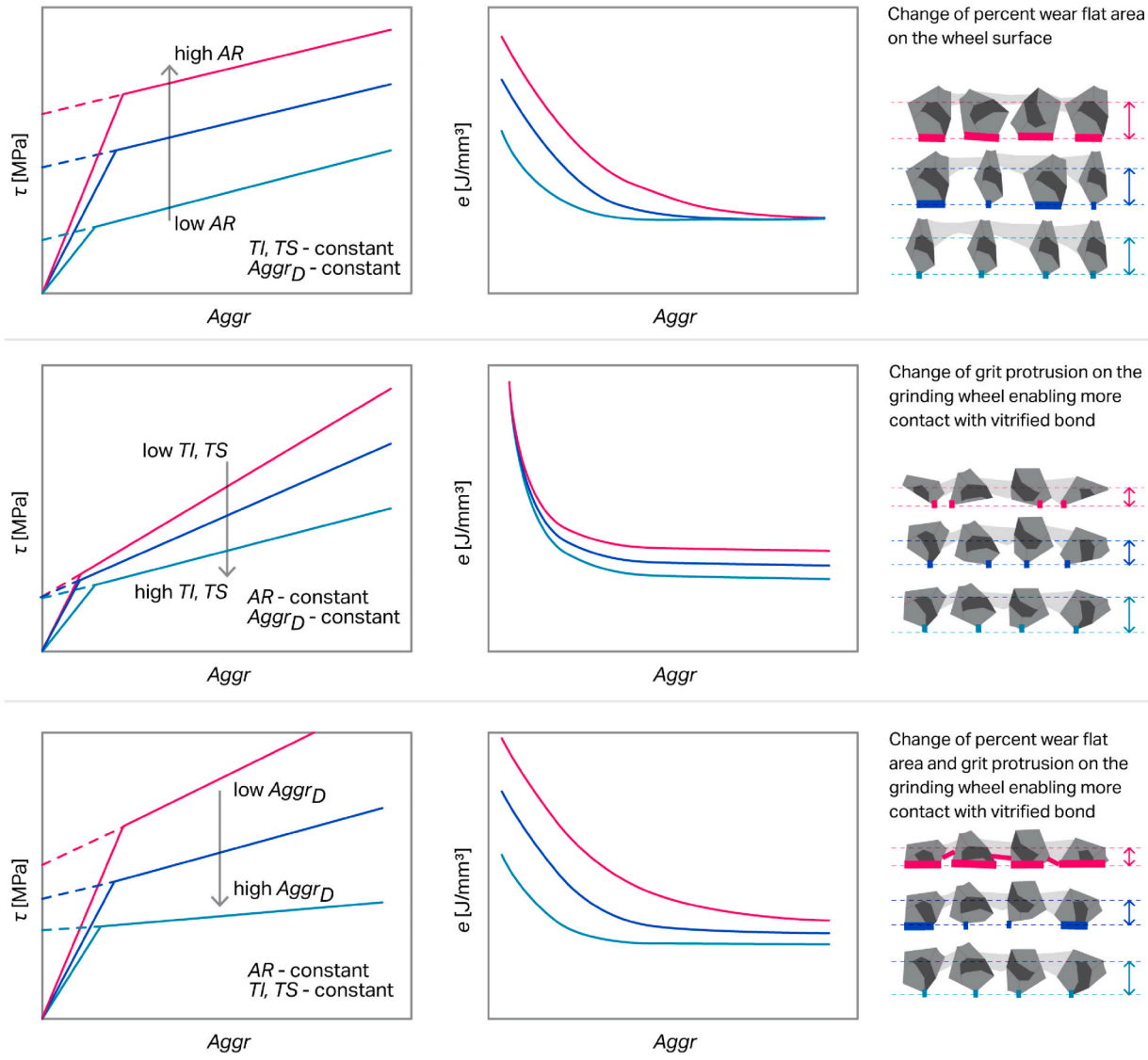
Fig. 17. Grinding-wheel responses. A conceptual depiction of grinding response and wheel performance for different grit properties (*TI*, *TS*, *AR*) and dressing conditions (*Aggr$_D$*). This framework can be utilised to foresee the theoretical performance changes of various grinding wheels dressed in different ways. The left column shows tangential stress vs. aggressiveness, the middle column shows specific energy vs. aggressiveness, and the right column illustrates wheel-workpiece interface in terms of percent of wear flat area *A* and grit protrusion *Δα*.

and grit properties; therefore, μ is also a good indicator of cutting efficiency.

- The sliding component of tangential stress τ_0 is affected by the grit aspect ratio *AR*, suggesting that grit shape has a first-order effect on the wear flat area.
- The grit protrusion, which is not usually considered in grinding wheel analysis, affects the intrinsic specific grinding energy.

Credit author statement

Nastja Macerol: Conceptualization, Methodology, Validation, Formal analysis, Investigation, Visualisation, Writing - original draft, Writing - review & editing, Resources, Project administration. **Luiz F.P. Franca**: Conceptualization, Methodology, Formal analysis, Investigation, Visualisation, Writing - original draft, Writing - review & editing. **Radovan Drazumeric**: Conceptualization, Methodology, Formal analysis, Investigation, Writing - review & editing. **Peter Krajnik**:

Conceptualization, Writing - review & editing, Supervision.

Declaration of competing interest

The authors declare that they have no known competing financial interests or personal relationships that could have appeared to influence the work reported in this paper.

Data availability

The data that has been used is confidential.

References

[1] A. Daneshi, N. Jandaghi, T. Tawakoli, Effect of dressing on internal cylindrical grinding, Proced. CIRP 14 (2014) 37–41, https://doi.org/10.1016/J.PROCIR.2014.03.064.

[2] S. Malkin, N.H. Cook, The wear of grinding wheels: part 1—attritious wear, ASME. J. Eng. Ind. 93 (1971) 1120–1128.

[3] S. Malkin, N.H. Cook, The wear of grinding wheels: Part 2—fracture wear, ASME. J. Eng. Ind. 93 (1971) 1129–1133.

[4] R. Cai, W.B. Rowe, Assessment of vitrified CBN wheels for precision grinding, Int. J. Mach. Tool Manufact. 44 (2004) 1391–1402, https://doi.org/10.1016/J.IJMACHTOOLS.2004.04.004.

[5] J.A. Badger, A.A. Torrance, A comparison of two models to predict grinding forces from wheel surface topography, Int. J. Mach. Tool Manufact. 40 (2000) 1099–1120, https://doi.org/10.1016/S0890-6955(99)00116-9.

[6] A.T. Nguyen, D.L. Butler, Correlation of grinding wheel topography and grinding performance: a study from a viewpoint of three-dimensional surface characterisation, J. Mater. Process. Technol. 208 (2008) 14–23, https://doi.org/10.1016/J.JMATPROTEC.2007.12.128.

[7] G. Garcia Luna, D. Axinte, D. Novovic, Influence of grit geometry and fibre orientation on the abrasive material removal mechanisms of SiC/SiC Ceramic Matrix Composites (CMCs), Int. J. Mach. Tool Manufact. 157 (2020), 103580, https://doi.org/10.1016/J.IJMACHTOOLS.2020.103580.

[8] A.J. Shih, An experimental investigation of rotary diamond truing and dressing of vitreous bond wheels for ceramic grinding, Int. J. Mach. Tool Manufact. 40 (2000) 1755–1774, https://doi.org/10.1016/S0890-6955(00)00022-5.

[9] M.P. Hitchiner, S.B. McSpadden, J.A. Webster, Evaluation of factors controlling CBN abrasive selection for vitrified bonded wheels, CIRP Ann. 54 (2005) 277–280, https://doi.org/10.1016/S0007-8506(07)60102-4.

[10] J. Palmer, D. Curtis, D. Novovic, H. Ghadbeigi, The influence of abrasive grit morphology on wheel topography and grinding performance, Proced. CIRP 77 (2018) 239–242, https://doi.org/10.1016/J.PROCIR.2018.09.005.

[11] E. Brinksmeier, M. Çinar, Characterization of dressing processes by determination of the collision number of the abrasive grits, CIRP Ann. 44 (1995) 299–304, https://doi.org/10.1016/S0007-8506(07)62330-0.

[12] S. Malkin, T. Murray, Mechanics of rotary dressing of grinding wheels, J. Eng. Ind. 100 (1978) 95–102, https://doi.org/10.1115/1.3439353.

[13] T. Murray, S. Malkin, Effects of rotary dressing on grinding wheel performance, J. Eng. Ind. 100 (1978) 297–302, https://doi.org/10.1115/1.3439425.

[14] R. Dražumerič, J. Badger, R. Roininen, P. Krajnik, On geometry and kinematics of abrasive processes: the theory of aggressiveness, Int. J. Mach. Tool Manufact. 154 (2020), 103567, https://doi.org/10.1016/J.IJMACHTOOLS.2020.103567.

[15] S. Malkin, C. Guo, Grinding technology: theory and applications of machining with abrasives, in: Grind. Technol. Theory Appl. Mach. With Abrasives, second ed., Industrial Press, New York, 2008, pp. 115–156.

[16] J. Badger, R. Dražumeric, P. Krajnik, Application of the dimensionless Aggressiveness number in abrasive processes, Proced. CIRP 102 (2021) 361–368, https://doi.org/10.1016/J.PROCIR.2021.09.062.

[17] N. Macerol, L.F.P. Franca, P. Krajnik, Effect of the grit shape on the performance of vitrified-bonded CBN grinding wheel, J. Mater. Process. Technol. 277 (2020), 116453, https://doi.org/10.1016/J.JMATPROTEC.2019.116453.

[18] J. Badger, Grinding of sub-micron-grade carbide: contact and wear mechanisms, loading, conditioning, scrubbing and resin-bond degradation, CIRP Ann. 64 (2015) 341–344, https://doi.org/10.1016/J.CIRP.2015.04.007.

[19] W. Le Zhu, A. Beaucamp, Compliant grinding and polishing: a review, Int. J. Mach. Tool Manufact. 158 (2020), 103634, https://doi.org/10.1016/J.IJMACHTOOLS.2020.103634.

[20] S. Malkin, N. Joseph, Minimum energy in abrasive processes, Wear 32 (1975) 15–23, https://doi.org/10.1016/0043-1648(75)90201-X.

[21] R. Snoeys, J. Peters, The significance of chip thickness in grinding, Ann. CIRP. 23 (1974) 227–237.

[22] J.M. Derkx, A.M. Hoogstrate, J.J. Saurwalt, B. Karpuschewski, Form crush dressing of diamond grinding wheels, CIRP Ann 57 (2008) 349–352, https://doi.org/10.1016/J.CIRP.2008.03.065.

[23] R.D. Monici, E.C. Bianchi, R.E. Catai, P.R. De Aguiar, Analysis of the different forms of application and types of cutting fluid used in plunge cylindrical grinding using conventional and superabrasive CBN grinding wheels, Int. J. Mach. Tool Manufact. 46 (2006) 122–131, https://doi.org/10.1016/J.IJMACHTOOLS.2005.05.009.

[24] Unified Abrasives Manufacturers' Association, For measuring-relative crystal strengths of diamond and cubic boron nitride grit, ANSI B74 23 (2002), 2002.

[25] M. Jackson, B. Mills, Hitchiner, Controlled wear of vitrified abrasive materials for precision grinding applications, Sadhana 28 (2003) 897–914.

[26] K. Breder, N. Corbin, P. Chinnakaruppan, S. Hartline, The influence of grinding conditions on the performance of different CBN types, Ind. Diam. Rev. (2005) 4–7.

[27] Federation of European Producers of Abrasives, FEPA Standards for Checking Superabrasives Grain Sizes, 2009, 2009, p. 61, 2009.

[28] Unified Abrasives Manufacturer's Association, Checking the size of diamond or cubic boron nitride abrasive products, ANSI B74. 16 (2002) 2002.

[29] Retsch Technology, Particle Size and Particle Shapeanalysis with Dynamic Image Analyser, 2015, pp. 1–12.

[30] M.C. Shaw, Principles of Abrasive Processing, Clarendon Press, 1996, in: https://global.oup.com/academic/product/principles-of-abrasive-processing-9780198590217#.YoY0o6fJxL8.mendeley. (Accessed 19 May 2022).

[31] M. Rasim, P. Mattfeld, F. Klocke, Analysis of the grain shape influence on the chip formation in grinding, J. Mater. Process. Technol. 226 (2015) 60–68, https://doi.org/10.1016/J.JMATPROTEC.2015.06.041.